Bulletin of Earthquake Engineering (2020) 18:6181–6201
https://doi.org/10.1007/s10518-020-00939-4

CASE STUDY REPORTS

A liquefaction case study of gently sloping gravelly soil deposits in the near-fault region of the 2008 M_w7.9 Wenchuan earthquake

Yan-Guo Zhou[1] · Peng Xia[1] · Dao-Sheng Ling[1] · Yun-Min Chen[1]

Received: 14 April 2020 / Accepted: 18 August 2020 / Published online: 28 August 2020

Abstract
The 2008 M_w7.9 Wenchuan earthquake in China caused widespread soil liquefaction and ground failures. A liquefaction case study of gently sloping ground at Yingxiu Town in the near-fault region is presented, which features its relatively thick deposits of sand-gravel mixtures, high soil stiffness, extremely intensive ground motion, large lateral spreading and severe damage of superstructure. The details of ground motion, site condition, field manifestations of liquefaction, subsurface soil profiles and field testing of shear wave velocities are presented. A conceptual binary mixture model is proposed to explain the gravel content effect on the stiffness and liquefaction resistance of gravelly soils. A preliminary liquefaction triggering evaluation method for gravelly soils is proposed by considering the gravel content correction of shear wave velocities based on the existing simplified procedure for typical sandy soils. The failure mechanism of the Baihua Bridge built at this site is explored, and the liquefaction-induced lateral spreading in down-slope direction might aggravate the failure process by imposing a large kinematic load on the piers besides the inertial forces transferred from the superstructure.

Keywords Liquefaction · Gravelly soils · Sloping ground · Shear wave velocity · Lateral spreading · Baihua Bridge · Case study · 2008 Wenchuan earthquake

✉ Yan-Guo Zhou
qzking@zju.edu.cn

Peng Xia
11612018@zju.edu.cn

Dao-Sheng Ling
dsling@zju.edu.cn

Yun-Min Chen
chenyunmin@zju.edu.cn

[1] MOE Key Laboratory of Soft Soils and Geoenvironmental Engineering, Institute of Geotechnical Engineering, Center for Hypergravity Experimental and Interdisciplinary Research, Zhejiang University, 866 Yuhangtang Rd., Zijingang Campus, Anzhong Bldg. B-404, Hangzhou 310058, P. R. China

1 Introduction

The May 12, 2008, M_w7.9 Wenchuan earthquake caused widespread soil liquefaction throughout a vast area of 500 km long and 200 km wide. One salient feature of liquefaction manifestations was the ejecta of gravelly soils, which were mainly distributed around Chengdu Plain where geologic setting typically consists of surface Holocene clayey soils and the underlying relatively thick gravelly soils (Zhou et al. 2009; Cao et al. 2011; Zhou et al. 2018). The liquefaction consequences of gravelly soils show significant differences compared with those of typical sands, and less ground deformation (e.g., settlement) and fewer surface ejecta were observed (Cetin et al. 2002; Wilkinson et al. 2013; Khoshnevisan et al. 2015). Although gravelly soils are commonly regarded as unlikely to liquefy and are widely used in the hydraulic dams, land reclamations and embankment engineerings (Hatanaka et al. 1997), the lessons from recent devasting earthquakes such as the 1995 Kobe earthquake and the 2016 Kaikoura earthquake urges a thorough understanding of the mechanism and evaluation of gravelly soils (e.g., Hatanaka et al. 1997; Ghafghazi et al. 2017a, b; Cubrinovski et al. 2017). Therefore, high-quality case studies of gravelly soils are of great interest, especially where failures of engineering structures built upon it were observed.

A liquefaction case study of gravelly soils that occurred in the near-fault region at Yingxiu Town is presented in this paper. This site is carefully investigated and the details of ground motion, site condition, field manifestations of liquefaction, subsurface soil profiles and field testing are presented. The grain size distribution curves of in-situ soils and the corresponding surface ejecta are compared, and a conceptual binary mixture model is proposed to illustrate the effect of gravel content on the stiffness and liquefaction resistance of gravelly soils. A preliminary liquefaction evaluation procedure for gravelly soils is proposed by considering gravel content correction of shear wave velocities based on the existing simplified procedure for typical sandy soils, which is then checked by this field case. The contribution of liquefaction-induced lateral spreading to the failure mechanism of the Baihua Bridge built at this site is discussed.

2 Field investigation and ground motion

2.1 Site description

The investigated site (103.477°E, 31.045°N, Elevation 854 m) is on the Minjiang floodplain, which locates about 2 km southwest to Yingxiu Town, Wenchuan County and has a distance of 12.7 km to the epicenter. Two boreholes (i.e., ZK3 and ZK5) were drilled on the left bank of the Minjiang River (see Fig. 1).

The Minjiang River zigzags successively across the test site and creates the floodplain with slopes ranging from 6.3 to 7.5%. Areas along the Minjiang River valley are mainly covered by fluvial deposits consisting of silty clay, gravelly soils and stiff bedrock from the surface to the bottom. The Baihua Bridge, once constructed in the southwest part of this site, was severely destroyed with some segments completely collapsed during the earthquake.

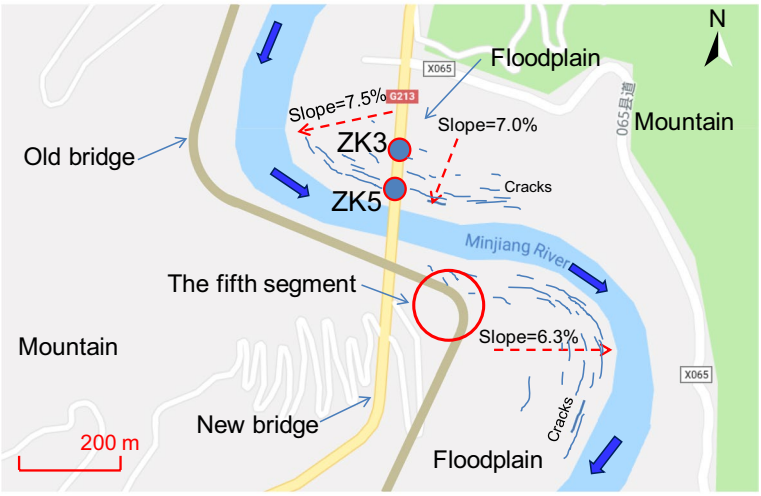

Fig. 1 Map of the investigated site at the Mingjiang floodplain

2.2 Estimation of ground motion

The peak ground motion of the investigated site was directly estimated from the ShakeMap of the 2008 Wenchuan earthquake contributed by ATLAS in 2017 (https://earthquake.usgs.gov/earthquakes/eventpage/usp000g650#shakemap) (see Fig. 2). The overall mapping philosophy of the ShakeMap is combining information from the individual stations, site amplification characteristics, and ground motion prediction equations to create the best composite map by considering the distance to the hypocenter (or to the causative fault).

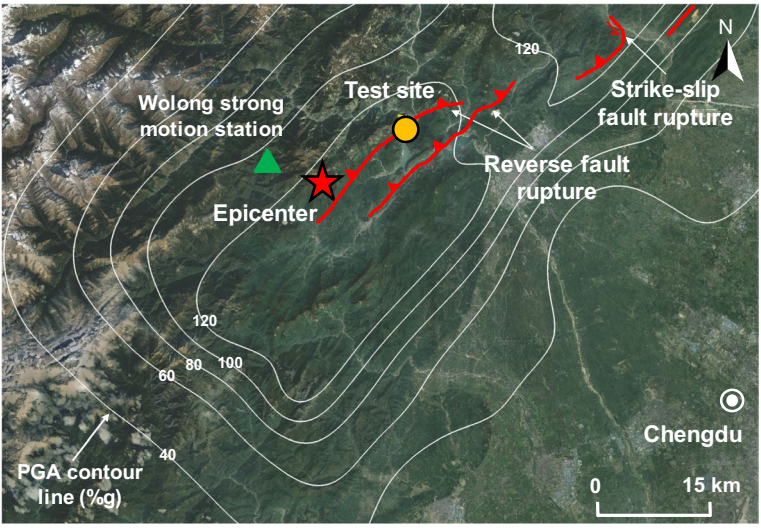

Fig. 2 The site location and ShakeMap of the 2008 Wenchuan earthquake

The mean and standard deviation of the peak ground acceleration (PGA) at the test site could be readily estimated according to the location coordinates, wherein the mean PGA at the test site was estimated to be 1.46 g with a deviation of 0.18 g.

The nearest strong motion station to the test site is Wolong Strong Motion Station (Code 51WCW, about 18 km to the site) and the recorded tri-directional acceleration time histories are shown in Fig. 3a. The resultant tri-directional acceleration path (see Fig. 3b) implies a complex loading path in the ground with large earthquake-induced cyclic shear stress and fast principal stress rotation. The Fast Fourier Transform (FFT) results indicate that the dominant frequencies are about 2 Hz and 5 Hz in EW and NS directions respectively (see Fig. 3c). As shown in Fig. 3d, the significant duration is about 52 s in the test site, which takes the time elapsed between 5 and 95% total integral of Arias intensity (Trifunac and Brady 1975). It could be found that the seismic energy released in the near-fault region is very intense, with the typical characteristics of large peak accelerations in all directions and large velocity pluses up to 0.5 m/s (Li et al. 2008b). Thus the consequent destructive effects of such ground motion were commonly severer than those in far-field regions.

2.3 Field manifestations of liquefaction

Due to the extremely high ground motion acceleration and long shaking duration, some spots of boiled gravelly soils and large surface deformation towards the Minjiang River

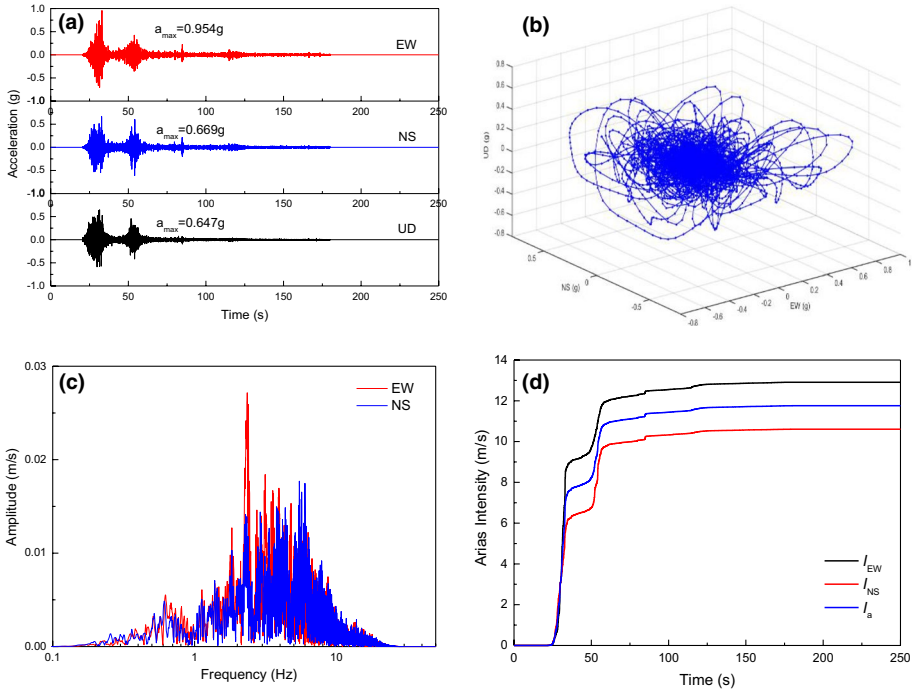

Fig. 3 Ground motion records at Wolong Station (51WCW): **a** tri-directional accelerations, **b** resultant acceleration paths, **c** FFT results and **d** Arias Intensity

were observed (see Fig. 4a). The crust layer of silty clay along the Minjiang River experienced moderate to large lateral spreading, resulting in many wide surface cracks with width up to 40 cm (see Fig. 4b, c). Along the riverbank, large lateral spreading could be found adjacent to the Baihua Bridge pier foundations, and the failure of the twin-column supporting pier and the girder falling off the bridge could be found in Fig. 4d, e. As shown in Fig. 4e, the liquefaction-induced relative movement between the pier foundation and the crust layer formed a gap of about 20 cm wide.

2.4 Subsurface soil conditions and field testing

In the field testing, core drilling was utilized to obtain the in-situ gravelly soils according to the *Chinese Code for Investigation of Geotechnical Engineering* (GB50021-2001, 2009), which will form a 104 mm-diameter hole (see Fig. 5a). Spectral analysis of surface wave (SASW) testing was conducted to measure the shear wave velocities (see Fig. 5b), and a sledge-hammer or a drop weight was used as the impact source according to the receiver spacing. The recording device was a CRAS Analyzer interfaced with a portable computer. Two geophones were used as receivers and different receiver distances were set at a given site. Detailed information on field SASW testing could be found in Zhou et al. (2009).

The investigated site is underlain by fluvial deposits (Q_4^{al+pl}) and boulders and weathered rock (T_{3X}). The subsurface soils are classified according to the Unified Soil Classification System (ASTM 2011), and gravelly sands with gravel content (GC) less than 50% belong to the sand division while sandy gravels with GC > 50% belong to the gravel division,

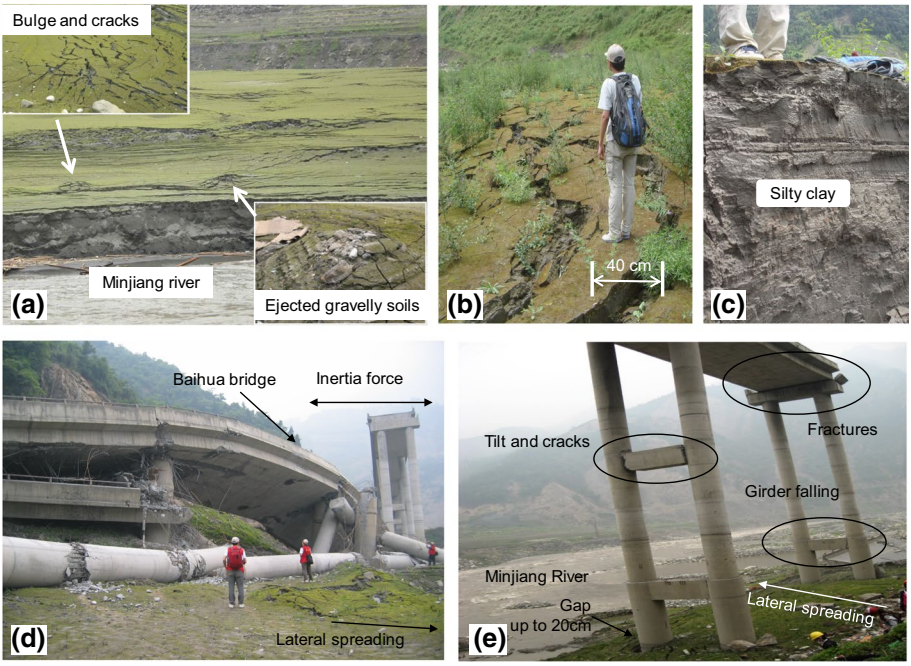

Fig. 4 Field manifestations: **a** ground cracks and soil boils, **b** large lateral spreading, **c** the crust layer of silty clay, **d** collapse of the Baihua Bridge and **e** pier damage details

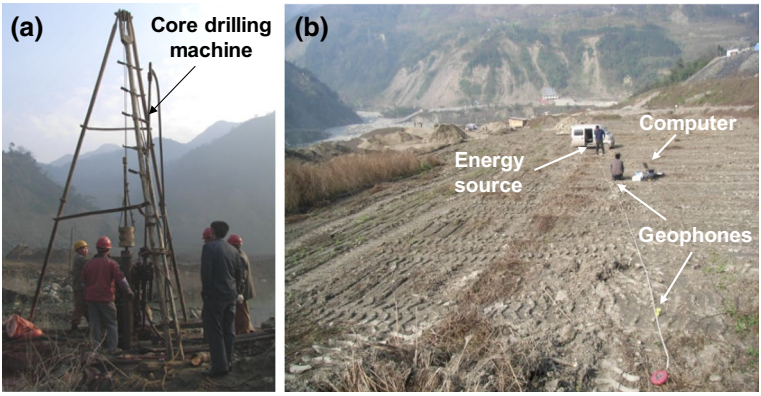

Fig. 5 Field testing: **a** borehole sampling and **b** SASW tests

where gravel refers to a soil with particle size ranging from 4.75 to 75 mm and sand is a soil with particle size ranging from 0.075 mm to 4.75 mm.

Take soil samples drilled from ZK3 as an example (see Fig. 6a), gravelly sand and sandy gravel layers are interbedded in shallow depth until larger cobbles and boulders and weathered rocks are encountered below the depth of 8.34 m. Figure 6b gives a profile view of 3-meter depth near ZK5. At ZK3 (see Fig. 7a), the 0.38 m-thick silty clay is underlain by a 3.19 m-thick layer of gravelly sands (GC = 40%). This gravelly sand layer is underlain by medium to coarse sands with gravelly sands (extends to 4.31 m, GC = 30%) and loose sandy gravels (extends to 8.34 m, GC ranges 60–80%) in sequence. At ZK5 (see Fig. 7b), the thickness of the crust silty clay layer is 0.6 m, underlain by a 2.6 m-thick layer of gravelly sands (GC = 40%). This gravelly sand layer is underlain by layers of medium sands with gravelly sands (extends to 4.2 m, GC = 30%) and medium dense sandy gravels (extends to 9.8 m, GC = 60–80%). Then boulders and weathered rocks are encountered.

The shear wave velocity measurements were conducted by the SASW tests in November, 2008. The measured shear wave velocities were converted to overburden stress-normalized values by using Eq. (1).

$$V_{s1} = V_s C_V = V_s \left(\frac{P_a}{\sigma'_v} \right)^{n/2}, \tag{1}$$

where C_v is the factor to correct field measured shear wave velocities for overburden stress σ'_v, and a maximum C_v value of 1.4 is applied at shallow depths (Idriss and Boulanger 2008); n is the power exponent in Hardin equation and usually takes 0.5; P_a is the atmospheric pressure and equals 101 kPa.

The V_s and V_{s1} profiles of ZK3 and ZK5 are shown in Fig. 7, where both profiles have higher V_s (i.e., high shear stiffness) compared with typical sandy soils. The high V_s could be explained by the inclusion of stiff gravel particles and the long depositing process. Cao et al. (2011) pointed out that the underlain gravelly soils in this region have deposited up to 6500–7500 years and it could be speculated that some aging effects like bonding or cementation among soil particles might have formed at natural state.

The criterion for selecting the critical layer in this study is to find the soil stratum that is the most likely to trigger and manifest liquefaction at the ground surface of a

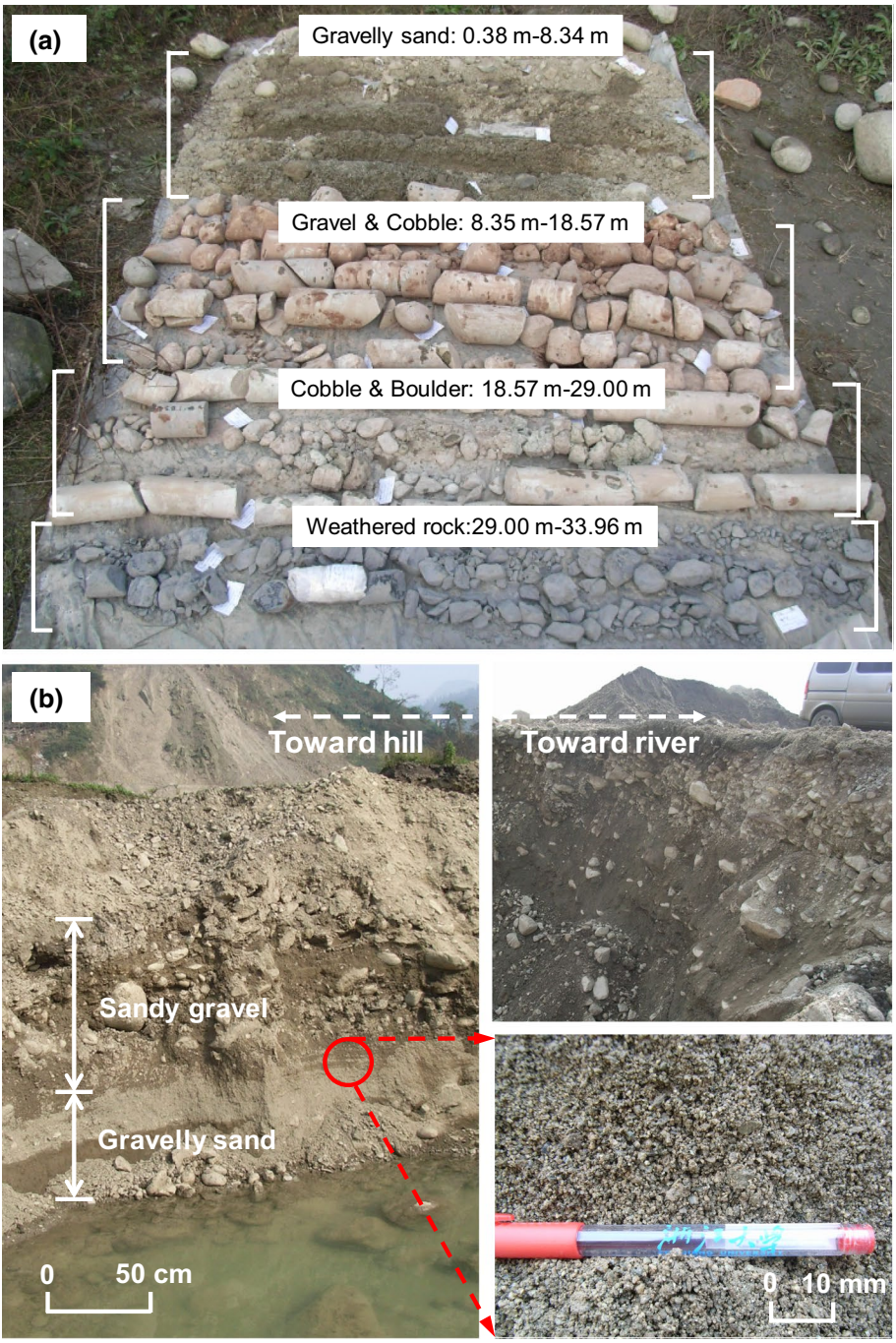

Fig. 6 Soil characteristics **a** soil sampling at ZK3; **b** an exposed soil strata near ZK5

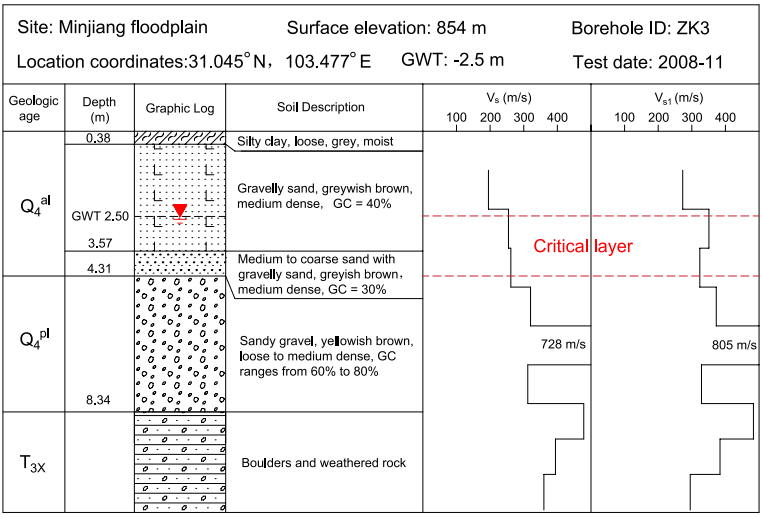

(a) ZK3

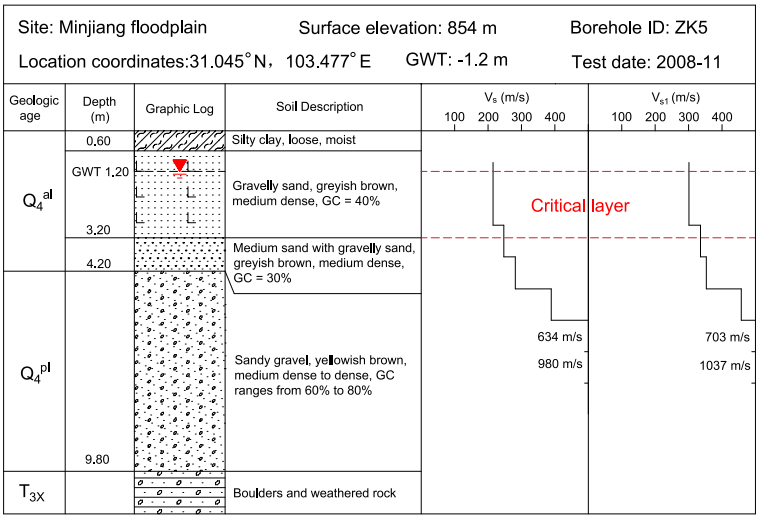

(b) ZK5

Fig. 7 The strata profiles and the shear wave velocity data: **a** ZK3 and **b** ZK5

given site (Zhou et al. 2020). Based on the soil strata and the V_{s1} profile, the critical layer of ZK3 is identified as the layers of loose gravelly sands and medium to coarse sands with gravelly sands, which could be evidenced by the ejected gravelly sands as shown in Fig. 4a. The critical layer depth varies from 2.5 m to 4.31 m and the average normalized shear wave velocity is 320 m/s. The most likely source of liquefaction in

ZK5 is the layer of gravelly sands. The critical layer depth varies from 1.2 m to 3.2 m and the average normalized shear wave velocity is 308 m/s.

3 Liquefaction evaluation of gravelly soils

3.1 Characteristics of the in-situ soils

Soil grain size distribution curves of the crust layer, the liquefiable layer of gravelly sands at 3 m depth, the non-liquefiable layer of sandy gravels at 7 m depth and the surface ejecta at ZK3 are all plotted in Fig. 8.

As shown in Fig. 8, the non-liquefiable sandy gravel layer mainly contains large-sized gravel particles, while the liquefiable gravelly sand layer contains fine to coarse particles as well as a small portion of gravel particles. The surface ejecta mainly consists of middle to fine particles as well as some gravel particles, and the crust layer mainly contains fine particles. This phenomenon indicates that a small portion of gravel particles from the gravelly sand layer were ejected and some fine-grained soils from the crust layer were also brought out by the upward movement of excess pore water during the liquefaction process (see Fig. 4a).

It could be found in Fig. 7 that the V_{s1} values in sandy gravel layers are usually larger than that in gravelly sand layers. To explain this phenomenon, a conceptual binary sand-gravel mixture model is proposed as shown in Fig. 9, where the schematic travel paths of shear waves in sands, gravelly sands, sandy gravels are illustrated and the corresponding propagation time of shear wave are t_1, t_2 and t_3, respectively. As noted by Chang (2016), the shear wave velocity of a water-saturated sandstone core (i.e., the analogue of gravel particles) ranges from 1580 to 3420 m/s, while the shear wave velocity of typical sandy soils is at the order of 150-250 m/s. According to Snell's law of elastic wave propagation, the upward propagation of the shear wave in clean sand sample is straight. For gravelly sands with low GC, the gravel particles are floating in the sand matrix and shear wave will take the priority to propagate through the gravel particles wherever possible. For sandy gravels with high GC, the gravel matrix has many force contacts and the shear wave mainly passes

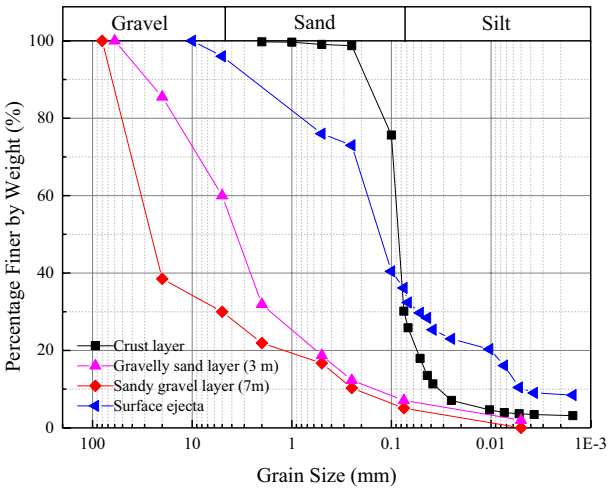

Fig. 8 Soil grain size distribution curves at ZK3

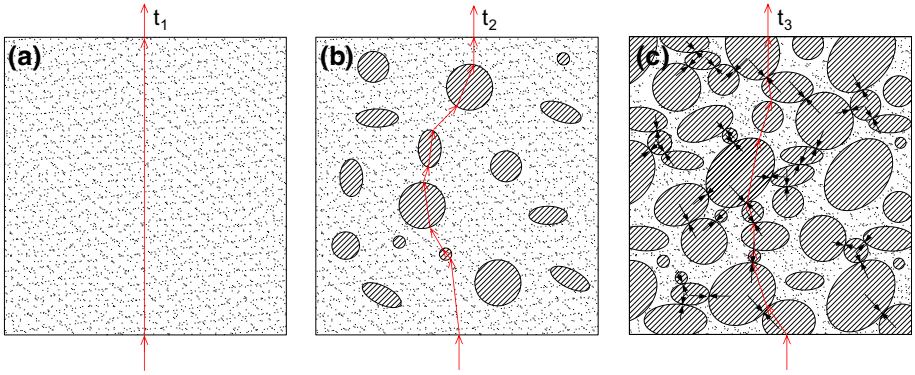

Fig. 9 Schematic of shear wave travel paths in sand-gravel mixtures: **a** clean sand; **b** gravelly sand and **c** sandy gravel

through the gravel particles, leading to high shear wave velocities. Thus it is expected that $t_1 > t_2 > t_3$ and the shear wave velocities of the gravelly soils will increase with the increased GC. Such a trend has also been reported by other researchers (e.g., Rollins et al. 1998; Modoni et al. 2000; Toyota and Takada. 2019). But it should be noted that besides the gravel content, several other factors including the maximum gravel particle size and relative density will also affect the shear wave velocity of gravelly soils.

From this conceptual model, it could be found that the gravelly sand soils are sand-dominant mixtures while the sandy gravel soils are gravel-dominant mixtures, which might significantly influence the dynamic behaviors. As shown in Fig. 9, the shear forces induced by dynamic loadings are supposed to be transmitted mainly by sand–sand contacts, sand-gravel contacts and gravel–gravel contacts, respectively. For a sand-gravel mixture, there is little to no gravel–gravel contacts due to the floating state of gravel particles when GC is less than some threshold value (e.g., GC = 30%), and the dynamic behavior is dominated by the sand matrix and the liquefaction resistance of gravelly sands is close to that of sands. While for sandy gravels with high GC, the strong gravel–gravel contacts are formed and the loose sand particles are filled in the voids of the gravel matrix, leading to high liquefaction resistance. This characteristic could be partly observed from the cyclic triaxial test results of gravelly soils (e.g., Evans and Zhou 1995; Toyota and Takada 2019). As shown in Fig. 10, the liquefaction resistance increases slightly when the GC is less than 30%, but it increases considerably when GC exceeds this threshold.

3.2 Liquefaction triggering evaluation of gravelly soils

The existing liquefaction triggering evaluation methods mainly apply for sandy soils (e.g., Andrus and Stokoe 2000; Zhou and Chen 2007; Kayen et al. 2013). As gravelly soils have high stiffness and high liquefaction resistance, the liquefaction potential of gravelly soils could not be directly evaluated by methods for typical sandy soils. Recently Chang (2016) revealed that the existence of gravel particles in a sand matrix would significantly increase the shear wave velocity of the sand-gravel mixtures while affecting the liquefaction resistance slightly, as long as the GC is less than some threshold value (say, 30–40%), because these gravel particles will be in a "floating" state in the sand matrix. By considering the effect of gravel content via the GC-corrected shear wave velocity, the liquefaction

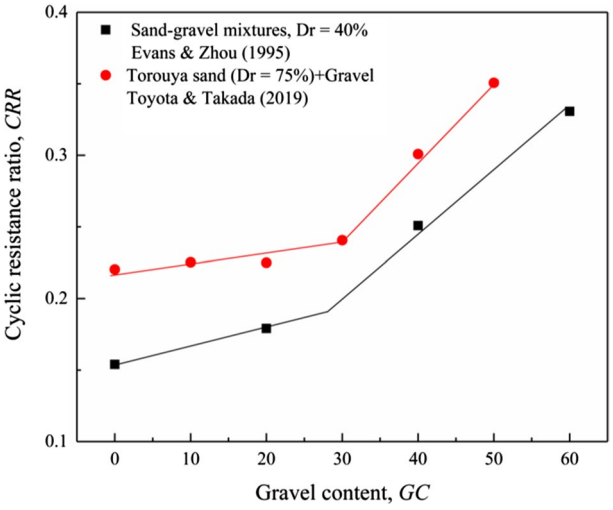

Fig. 10 The relationship between gravel content and cyclic resistance ratio

evaluation of gravelly soils could be converted to the evaluation of the corresponding sand matrix. Thus a preliminary liquefaction evaluation method for gravelly soils with low GCs is proposed based on field measurement of shear wave velocities, and it also takes the initial shear stress effect into account by relating the liquefaction resistance to the relative state parameter index of the corresponding sand matrix (e.g., Boulanger 2003; Flora et al. 2012). It is briefly introduced as follows:

Step 1: Calculate the GC-corrected shear wave velocity by using Eq. (2).

$$\frac{V_{s1,sk}}{V_{s1}} \simeq 1 - \frac{b}{1+e} \cdot GC, \tag{2}$$

where $V_{s1,sk}$ is the overburden stress-corrected GC-corrected shear wave velocity for the sand matrix; V_{s1} is the overburden stress-corrected shear wave velocity of the sand-gravel mixtures; b is the effective contact ratio, which represents the portion of the gravel particles that contribute to the active interparticle contacts and equals to 0.65 (Chang, 2016); e is the void ratio of the sand-gravel mixtures.

Step 2: Simplify the field condition into an infinite slope as shown in Fig. 11, and calculate the initial shear stress ratio (α) by using Eq. (3), which was modified from Mello and Pratson (1999).

$$\begin{cases} \alpha = \frac{\tau}{\sigma'} \\ \sigma' = \frac{2\cos 2\theta}{1+\cos 2\theta - K_0(1-\cos 2\theta)} \left(\sum_{i=1}^{n} \gamma_i' \Delta h_i \right) \cos^2 \theta + \frac{2\sin 2\theta}{1+\cos 2\theta - K_0(1-\cos 2\theta)} \cdot \frac{1}{2} \left(\sum_{i=1}^{n} \gamma_i' \Delta h_i \right) \sin 2\theta \\ \tau = \frac{(K_0-1)\sin 2\theta}{1+\cos 2\theta - K_0(1-\cos 2\theta)} \left(\sum_{i=1}^{n} \gamma_i' \Delta h_i \right) \cos^2 \theta + \frac{1+K_0+(1-K_0)\cos 2\theta}{1+\cos 2\theta - K_0(1-\cos 2\theta)} \cdot \frac{1}{2} \left(\sum_{i=1}^{n} \gamma_i' \Delta h_i \right) \sin 2\theta \end{cases} \tag{3}$$

where σ' is the vertical effective stress at the depth in question; τ is the initial shear stress acting on the horizontal plane; θ is the inclination angle of the site; K_0 is the coefficient of static earth pressure and equals 0.5 in this study; γ'_i is the effective density of each layer; Δh_i is the thickness of each layer.

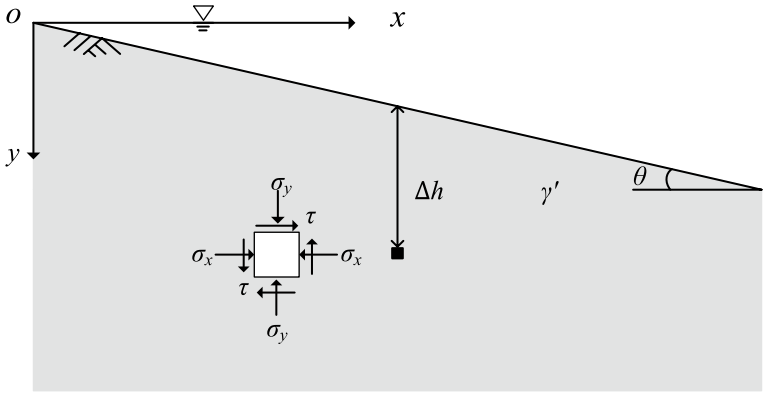

Fig. 11 The stress state of a soil element in an infinite slope

Step 3: Calculate the correction factor K_α by using Eq. (4), which was proposed by Boulanger (2003).

$$\begin{cases} K_\alpha = a + b \cdot \exp\left(\frac{-\xi_R}{c}\right) \\ a = 1267 + 636\alpha^2 - 634 \cdot \exp(\alpha) - 632 \cdot \exp(-\alpha) \\ b = \exp[-1.11 + 12.3\alpha^2 + 1.31 \cdot \ln(\alpha + 0.0001) \\ c = 0.138 + 0.126\alpha^2 + 2.52\alpha^3 \end{cases}, \tag{4}$$

where ξ_R is a relative state parameter index, which empirically relates the relative density and stress state for clean sands and could be expressed as Eq. (5).

$$\xi_R = \frac{1}{Q - \ln\left(\frac{100p'}{P_a}\right)} - D_r, \tag{5}$$

where p' is the effective confining stress; D_r is the relative density; Q is an empirical constant and approximately equals to 10 for quartz. In consideration of the essence of the proposed method to evaluate the liquefaction resistance of the sand matrix, the relative state parameter for clean sands could be used for the sand matrix in question.

Step 4: Calculate the liquefaction resistance ($CRR_{Mw=7.5}$) of the sand matrix based on the field measurement of shear wave velocities. For example, the following *CRR* -V_{s1} correlation with parameters of the best-fit curve is used to predict the *CRR*, which was originally proposed by Zhou and Chen (2007) based on laboratory tests of various sandy soils.

$$CRR_{M_w=7.5} = K_\alpha r_c \frac{1}{P_a}\left[\frac{k_{15}\rho}{F(e_{\min})}\right]^2 (V_{s1,sk})^4, \tag{6}$$

where r_c is a constant value accounting for the effect of multidirectional shakings (=0.9–1.0); k_{15} is the fitting value for a given failure cyclic number 15 from cyclic triaxial tests; $e_{\min}$ is the minimum void ratio of the soil; $F(e)$ is void ratio function and could be expressed as $F(e) = 1/(0.3 + 0.7e^2)$; ρ is the total mass density of the soil.

Step 5: Calculate the earthquake-induced cyclic stress ratio (*CSR*) by using Eq. (7).

$$CSR = 0.65\left(\frac{a\max}{g}\right)\left(\frac{\sigma_v}{\sigma'_v}\right)r_d, \tag{7}$$

where $a_{\max}$ is the peak horizontal ground surface acceleration (PGA) in unit of gravity; g is the acceleration of gravity; σ_v is the total overburden stress at the depth in question; and r_d is the shear-mass participation parameter to adjust for the flexibility of the soil profile, which could be expressed as Eq. (8) (Idriss and Boulanger 2006).

$$\begin{cases} r_d = \exp(\alpha(z) + \beta(z)M_w) \\ \alpha(z) = -1.012 - 1.126\sin(z/11.73 + 5.133) \\ \beta(z) = 0.106 + 0.118\sin(z/11.28 + 5.142) \end{cases}, \tag{8}$$

where z is the depth below ground surface in meters.

Then a magnitude scaling factor (MSF) is applied to obtain the equivalent $CSR_{M\mathrm{w}=7.5}$ for $M_{\mathrm{w}}=7.5$ by using Eq. (9).

$$\begin{cases} CSR_{M_w=7.5} = \frac{CSR}{MSF} \\ MSF = 6.9\exp\left(-\frac{M_w}{4}\right) - 0.058 \end{cases}, \tag{9}$$

Step 6: Calculate the safety factor of liquefiable layers in question by using Eq. (10).

$$F_s = \frac{CRR_{M_w=7.5}}{CSR_{M_w=7.5}}, \tag{10}$$

For this test site, the inclination angle θ for calculation takes an average value of 4°, and the relative density of the sand matrix is estimated to be 60–70%. The corresponding K_α changes from 1.03 to 1.01 for the soil depth from 1.5 m to 8 m, and it implies that the initial shear stress acting on this gently sloping ground would increase the liquefaction resistance slightly compared to that of the level ground. As suggested by Zhou and Chen (2007), the parameters to calculate the field CRR of silica sand in an average way are adopted as: $r_{\mathrm{c}}=0.9$, $k_{15}=1.387\times10^{-4}$ kPa$^{-0.5}$, $e_{\min}=0.65$, $\rho=1.90$ Mg/m^3. Based on these parameters, the estimated F_{s} for each layer at ZK3 and ZK5 are given in Fig. 12. Also, another set of calculations according to the probabilistic analysis of the global catalog of V_{s}-based liquefaction case histories (e.g., Kayen et al. 2013) is plotted in Fig. 12 for comparison purpose, where CRR is determined according to the probabilistic CRR-V_{s1} curve of $P_{\mathrm{L}}=50\%$ corresponding to $F_{\mathrm{s}}=1.0$.

As shown in Fig. 12, despite the slight differences between these two estimations, they both tell the same thing that the liquefied layer of the test site is shallow and the thickness is limited, and the liquefaction would be marginal to moderate as the factor of safety is below but close to 1. It explains the reason why there were only a few sand-gravel ejecta and limited lateral spreading and settlement at this site even under such violent ground shaking. Note that the GC-corrected shear wave velocities ($V_{\mathrm{s1,sk}}$) at the critical layers are around 250 m/s and much higher than that of typical liquefiable sandy soils, which could be explained by two possible reasons: the first is, the parameters used in Eqs. (1) and (2) for correcting shear wave velocities are for general conditions instead of site-specific, which would lead to some deviations; the second is, the proposed method in Step 1 to correct the GC effect on V_{s} was developed based on laboratory tests of reconstituted samples, which might have some limitations for field conditions in consideration of the wide range

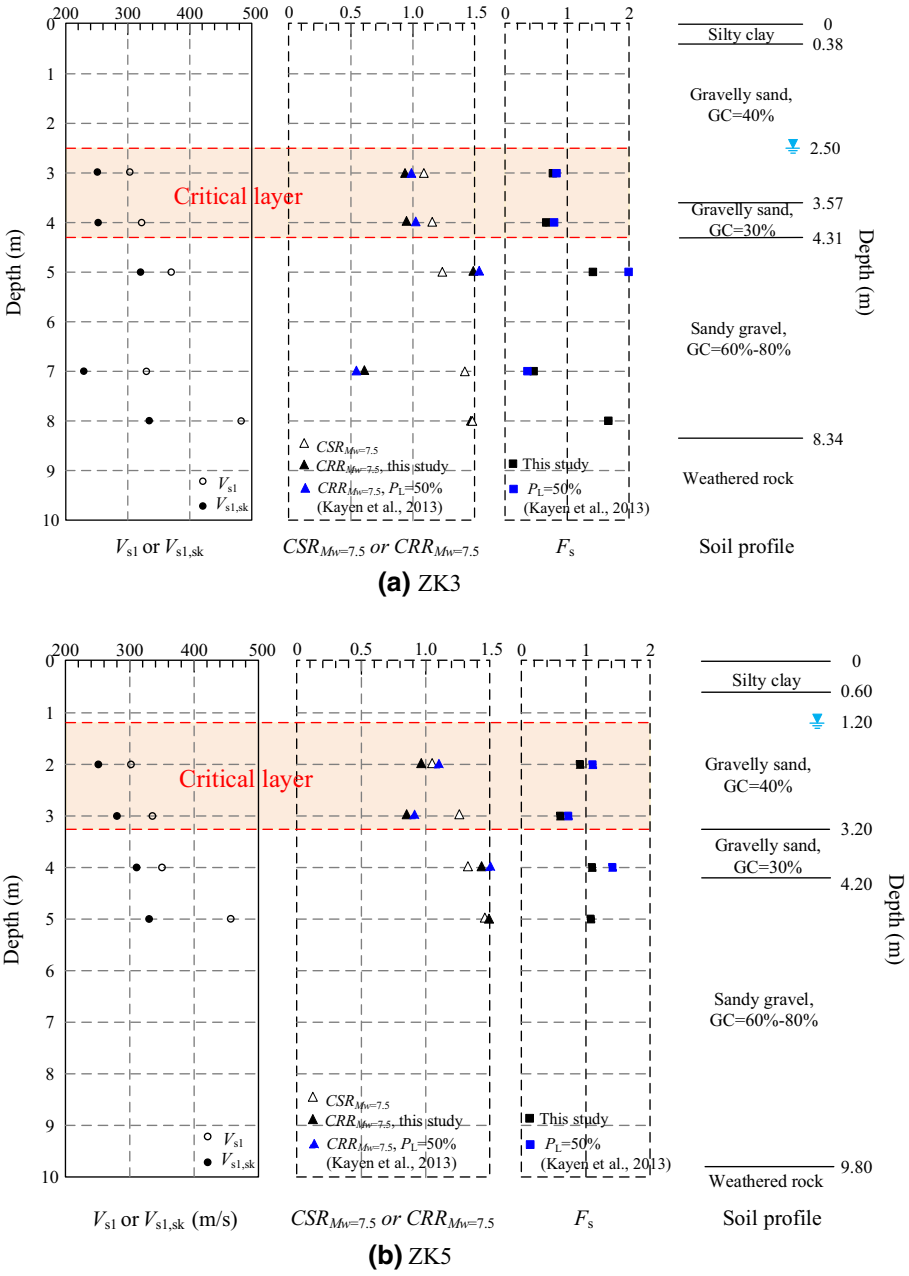

Fig. 12 Liquefaction evaluation of the test site: **a** ZK3; **b** ZK5

of gravel contents and the complex seismic and geologic histories. Other important features such as the inclusion of large gravel particles and even soil cementation between soil particles in the field deposits could be further considered to potentially improve the prediction performance of the present preliminary method. Besides, the datasets from this case

study could be added to the worldwide liquefaction database and benefit the deterministic and probabilistic liquefaction triggering evaluation methods for gravelly soils (e.g., Cao et al. 2011; Hubler 2017).

3.3 Liquefaction-induced lateral spreading

The effects of boundary condition and initial stress state on liquefaction-induced lateral spreading of sand deposits were studied in previous research. As for the effect of the impermeable crust layer, Fiegel and Kutter (1994) found from the centrifuge shaking table tests that the mildly sloping ground model with capped silt showed concentration of lateral displacement and reduction in the sliding resistance at the interface. Kamai and Boulanger (2013) conducted numerical simulations and found that the model layered part suffered enhanced lateral deformation. As for the effect of initial static shear stress on inclined ground, Yang and Sze (2011) revealed that the sloping sites would suffer much larger shear strain when subjected to cyclic shaking and cause extensive distortions of the subsoil and large lateral spreading in field conditions. These findings are helpful to understand the liquefaction-induced lateral spreading at the test site.

As shown in Fig. 13, the upward excess pore water pressure transmission will be retarded around the interface due to the impermeable crust layer of silty clay at the test site, which would lead to the large accumulation of volumetric strain and a substantial reduction of liquefaction resistance of the underlying liquefiable gravelly sands. Once the residual shear strain accumulated enough to crack the crust layer, the underlying sand and some of the floating gravel particles in the loosen sand-gravel mixtures will be gushed out with the upward pore water drainage while most of the underlain gravel matrix remains stable. Therefore the liquefaction-induced settlement was not so severe at the test site, because the ejecta were of small amount and most of the gravel particles were still buried underneath. This observation is similar to the cases of embankment failure during the 1988 Armenia earthquake (Yegian et al. 1994), where the 30 cm-thick impermeable crust layer impeded drainage and caused liquefaction-induced lateral spreading of gravelly soils. It will be

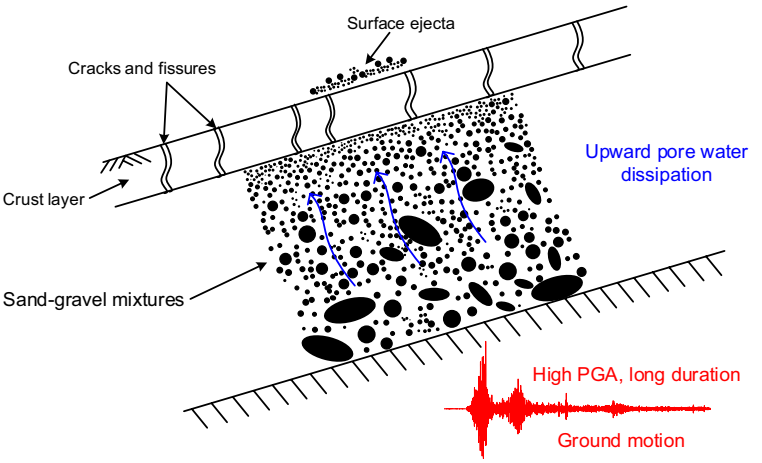

Fig. 13 Liquefaction mechanism of a sloping gravelly soil deposit

interesting to study the drainage conditions on liquefaction hazards of gravelly soils by physical modeling or numerical analysis in future study.

As the flow-type failure was not observed in this test site, the residual strength of the liquefied gravelly sands was expected to be moderate. The gravelly sand layer would accumulate strain under the cyclic shear stress induced by the earthquake. Many monotonic triaxial tests have indicated that the residual strength at $\gamma = 5$–7% of sand-gravel mixtures was close to the peak ones (Fioravante et al. 2012; Hubler et al. 2017). So the residual strength of the gravelly sands could be approximately back-calculated by combining the initial shear stress and the peak horizontal dynamic stress induced by the earthquake in the downslope direction. In this case, the average crust layer of the test site is about 0.5 m and the peak ground acceleration is 1.46 ± 0.18 g, which leads to the total shear stress about 12–15 kPa at the bottom of the crust layer, then the corresponding residual strength is back calculated as the equivalence. The estimated residual strength is close to that of gravelly sands estimated by SPT tests in the 1988 Armenia earthquake (Yegian et al. 1994) and that of the clean sands by SPT tests in the 1971 San Fernando earthquake (Seed et al. 1989). This finding indicates that the liquefied gravelly sands have similar behavior compared with that of the clean sands as the gravel particles are floating in the sand matrix.

4 Liquefaction effect on the failure of the Baihua Bridge

4.1 Brief description of the Baihua Bridge

The 495.55 m-long Baihua Bridge was constructed on the National Highway 213 in 2004. The bridge had six segments above this site and only the two damaged segments (i.e., the fifth and the sixth ones) are sketched in detail in Fig. 14. The location of the fifth segment is also marked in Fig. 1, which consisted of 23 m × 5 RC continuous spans and had a 66 m radius of the line curvature. The fifth segment was adjacent to the abutment, and the pier heights within this segment ranged from 18.1 m to 30.3 m, resulting in big stiffness differences between these piers. The fifth segment collapsed completely towards the mountainside during the earthquake (see Fig. 4(d) and 4(e)) while the lateral braces of other segments were heavily damaged due to the dynamic interactions between the piers and the girders. The sixth segment was supported by bilateral sliding bearings on the abutment and a fixed bearing on the middle pier. The curved fifth segment was supported by only one fixed bearing in the middle pier and the south end was seated on an in-span hinge about 1.7 m from the end pier of the sixth segment (Li et al. 2008a).

In bridge design, the girder is usually set inclined towards the mountainside for driving stability according to the radius of the line curvature. As shown in Fig. 15, two supporting piers of the fifth segment were uneven and the one towards the mountainside was a little shorter. Taking the middle piers of the fifth segment as an example, the 1.4 m-thick box-girder was supported by the 30 m-tall moment-resisting frame piers, which consisted of two circular reinforced concrete columns and lateral beams. The 800 mm-diameter piers were embedded in a sloping ground consisting of layers of silty clay, liquefiable gravelly soils, non-liquefiable gravelly soils and bedrock. Some possible failure mechanisms were explored from the perspective of ground shaking direction and structure design problems (e.g., Han et al. 2009; Kawashima et al. 2009). Another possible failure mechanism from the viewpoint of liquefaction is discussed, where the effect of kinematic forces on the piers from the lateral spreading is emphasized.

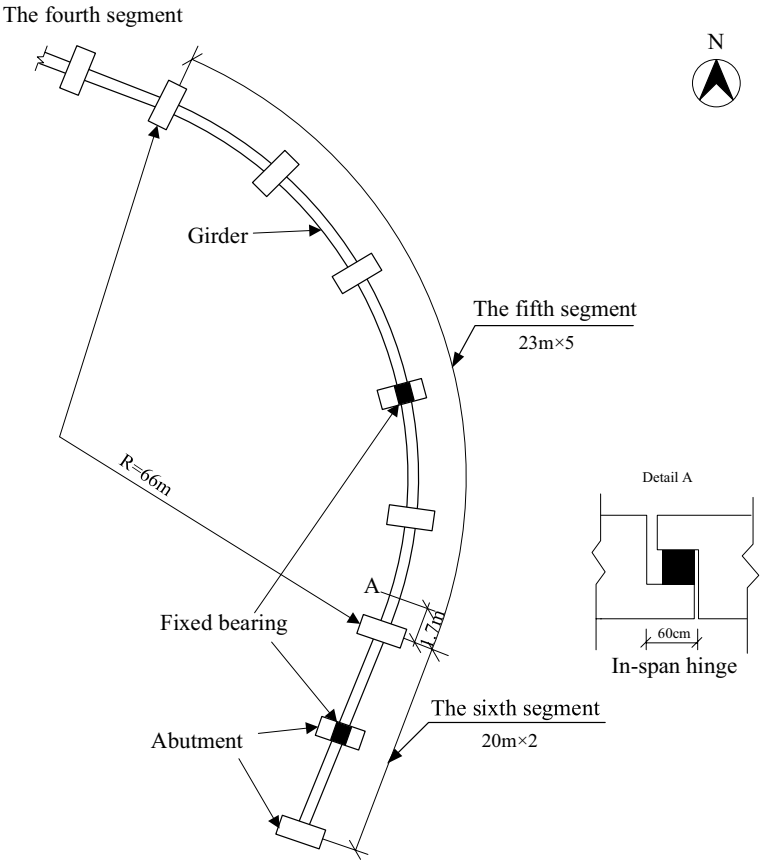

Fig. 14 Plan view of the segments of the Baihua Bridge (modified from Li et al. (2008a))

4.2 Kinematic forces on the piers from the lateral spreading

During the earthquake, the liquefaction-induced large lateral spreading occurred due to the long intensive ground shaking, and such downslope movement of soil layers will impose large kinematic forces on the piers. So it is important to take the soil-pile interactions in liquefiable soils into account to depicture the failure process, rather than only considering the dynamic responses of the superstructures.

As detailed information of the in-situ soils and the bridge are not available for analysis, the centrifuge model test conducted by Brandenberg et al. (2005) could give some reasonable insight into the soil-structure dynamic interactions. Consequently, liquefaction would induce large relative displacement between the crust layer and the underlain loose gravelly sand layer. But the further downslope movement of the crust layer was stopped by the pile. In return, the lateral driving loads acting on the piles by the crust layer and the liquefiable sand layer could aggravate the tilting tendency of the piles. Because the test site has almost identical soil strata and ground inclination as the model ground reported by Brandenberg et al. (2005), the lateral driving loads acting on the piers could be estimated by proportional interpolation according to the centrifuge test results, where the peak base

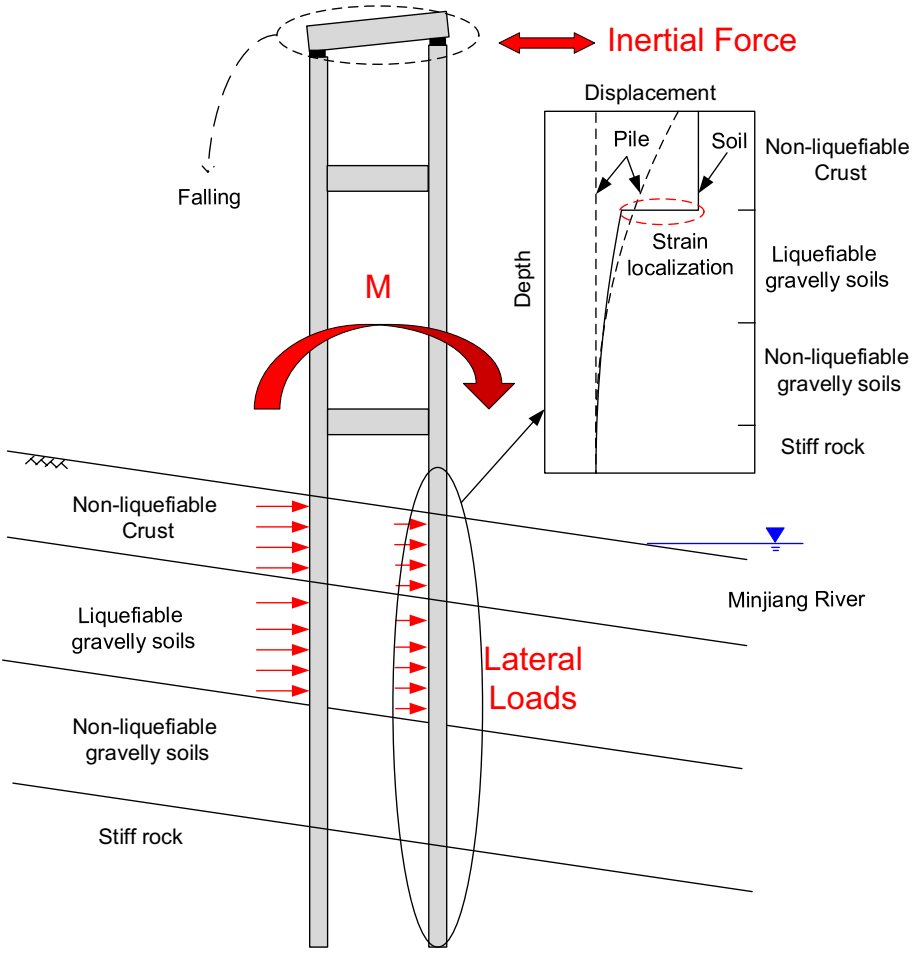

Fig. 15 A possible failure mechanism of the Baihua Bridge

acceleration is 0.69 g and the crust layer has a thickness of 2.5 m at prototype scale. In view of the extremely intensive ground motion (PGA = 1.46 g in EW direction) and the 0.5 m-thick crust layer at the site, a conservative approximation of the lateral driving loads imposed by the crust layer and the underlain liquefiable layer are about 100 kN and 110 kN/m respectively. These lateral loads would superimpose the inertia force from the girder (see Fig. 15), which might result in a large magnitude of bending moment and even large torque. Some piers might directly collapse under this large and complex loads, causing the girder violently falling towards the mountainside (see Fig. 4d). Many cracks on the lateral beams could be observed, and even some lateral beams were detached from the columns at the joints (see Fig. 4e). Another consequence of these lateral loads was the large tilt and drift of the piers. Since the girders and piers were not rigidly connected, the girder moved and dislodged off the supporting piers due to the excessive lateral displacement.

It could be preliminarily concluded that the liquefaction-induced lateral spreading of a sloping ground might aggravate the bridge failure process by imposing a large horizontal kinematic load in the downslope direction. It is interesting to note in Fig. 1 that the

newly-designed Baihua Bridge tries to avoid the possible lateral driving force by crossing the line perpendicular to the Minjiang River, which could also minimize the stiffness differences between the supporting piers. It is recommended to further carry out model tests or numerical analysis to reveal the effect of soil liquefaction on bridge failure mode (e.g., Bouckovalas and Chaloulos 2014), and shed light on the development of the resilient seismic design of bridges built upon sloping liquefiable grounds.

5 Conclusions

A liquefaction case study of gently sloping gravelly soils during the 2008 Wenchuan earthquake is carried out in this study. The test site features the sand-gravel mixtures, high soil stiffness, initial static shear stress, extreme intensive ground motion, and severe superstructure damage. The details of ground motion, site description, subsurface soil conditions and field testing are presented. The liquefaction mechanism and evaluation of gravelly soils are studied, and the related failure mechanism of the Baihua Bridge is also explored. The main findings are drawn as follows:

1. The impermeable crust layer of silty clay will retard the upward transmission of excess pore water pressure, resulting in the high concentration of volumetric strain at the interface and substantial liquefaction resistance reduction of the underlying liquefiable gravelly sands. The comparison of the grain size distribution curves of the in-situ soils and the surface ejecta indicates that a small portion of underlain gravel particles and some fine-grained soils were gushed out by the upward movement of excess pore water during the liquefaction process. The liquefaction-induced settlement is not so severe at this test site because most of the underlain gravel matrix remains stable.
2. A binary mixture model is proposed to explain the effect of gravel content on the stiffness and liquefaction resistance of gravelly soils. The inclusion of gravel particles will significantly increase the shear wave velocity of the soil. However from the perspective of soil force chains, the gravelly soils will be sand-like and have liquefaction resistance comparable to that of typical sands when GC is less than the threshold value. A preliminary liquefaction evaluation method for gravelly soils is proposed and checked by this case study, which employs the GC-corrected shear wave velocity and typical V_s-based procedure for sands with further consideration of the effect of initial shear stress. It is found that the initial shear stress acting on this gently sloping ground would increase the liquefaction resistance slightly compared to that of the level ground.
3. The liquefaction-induced lateral spreading of a sloping site might aggravate the failure process of Baihua Bridge by imposing a large horizontal kinematic load. The conservatively estimated lateral driving loads imposed by the crust layer and the underlain liquefiable layer could be about 100 kN and 110 kN/m respectively. The combination of kinematic loads and the inertial force transferred from the superstructure would lead to a large magnitude of bending moment and even large torque. The large and complex loading process might directly cause the collapse of the supporting piers, and excessive lateral displacement of the supporting piers induced by the tilt and drift of the piers were also expected.

Acknowledgements This study is supported by the National Natural Science Foundation of China (Nos. 51778573, 51978613, 51988101), the Chinese Program of Introducing Talents of Discipline to University

(the 111 Project, No. B18047) and the Science Technology Department of Zhejiang Province (Centrifugal Hypergravity and Interdisciplinary Experiment Facility, CHIEF). The authors would thank Dr. Chao Han and Dr. Hongguang Jiang for their kind help during the field investigations.

References

Andrus RD, Stokoe KHII (2000) Liquefaction resistance of soils from shear-wave velocity. ASCE J Geotech Geoenviron Eng 126(11):1015–1025

ASTM (2011) Standard Practice for Classification of Soils for Engineering Purposes (Unified Soil Classification System). ASTM International

Bouckovalas G, Chaloulos Y (2014) Kinematic interaction of piles in laterally spreading ground. Bull Earthq Eng 12(3):1221–1237

Boulanger RW (2003) Relating Kα to relative state parameter index. ASCE J Geotech Geoenviron Eng 129(8):770–773

Brandenberg SJ, Boulanger RW, Kutter BL, Chang D (2005) Behavior of pile foundations in laterally spreading ground during centrifuge tests. ASCE J Geotech Geoenviron Eng 131(11):1378–1391

Cao ZZ, Youd TL, Yuan XM (2011) Gravelly soils that liquefied during 2008 Wenchuan, China earthquake, Ms = 8.0. Soil Dyn Earthq Eng 31(8):1132–1143

Cetin KO, Youd TL, Seed RB, Bray JD, Sancio R, Lettis W, Yilmaz MT, Durgunoglu HT (2002) Liquefaction-induced ground deformations at Hotel Sapanca during Kocaeli (Izmit), Turkey earthquake. Soil Dyn Earthq Eng 22(9–12):1083–1092

Chang WJ (2016) Evaluation of liquefaction resistance for gravelly sands using gravel content–corrected shear-wave velocity. ASCE J Geotech Geoenviron Eng 142(5):04016002

Cubrinovski M, Bray J, De TC, Olsen MJ, Bradley BA, Chiaro G, Stocks E, Wotherspoon L (2017) Liquefaction effects and associated damages observed at the Wellington Centreport from the 2016 Kaikoura earthquake. Bull New Zeal Soc Earthq Eng 50(2):152–173

Evans MD, Zhou S (1995) Liquefaction behavior of sand-gravel composites. ASCE J Geotech Eng 121(3):287–298

Fiegel GL, Kutter BL (1994) Liquefaction-induced lateral spreading of mildly sloping ground. ASCE J Geotech Eng 120(12):2236–2243

Fioravante V, Giretti D, Jamiolkowski M, Rocchi G (2012) Triaxial tests on undisturbed gravelly soils from the Sicilian shore of the Messina Strait. Bull Earthq Eng 10(6):1717–1744

Flora A, Lirer S, Silvestri F (2012) Undrained cyclic resistance of undisturbed gravelly soils. Soil Dyn Earthq Eng 43:366–379

GB50021-2001 (2009) Chinese Code for Invetigation of Geotechnical Engineering. Ministry of Construction of the People's Republic of China

Ghafghazi M, DeJong JT, Sturm AP, Temple CE (2017a) Instrumented Becker Penetration Test, II: iBPT-SPT correlation for liquefaction assessment in gravelly soils. ASCE J Geotech Geoenviron Eng 143(9):04017063

Ghafghazi M, DeJong JT, Wilson D (2017b) Review of Becker Penetration Test interpretation methods for liquefaction assessment in gravelly soils. Can Geotech J 54(9):1272–1283

Han Q, Du X, Liu J, Li ZX, Li LY, Zhao JF (2009) Seismic damage of highway bridges during the 2008 Wenchuan earthquake. Earthq Eng Eng Vib 8(2):263–273

Hatanaka M, Uchida A, Ohara J (1997) Liquefaction characteristics of a gravelly fill liquefied during the 1995 Hyogo-Ken Nanbu earthquake. Soils Found 37(3):107–115

Hubler JF (2017). Laboratory and In-situ Assessment of Liquefaction of Gravelly Soils. Ph.D. Dissertation, University of Michigan

Hubler JF, Athanasopoulos-Zekkos A, Zekkos D (2017) Monotonic, cyclic, and postcyclic simple shear response of three uniform gravels in constant volume conditions. ASCE J Geotech Eng 143(9):04017043

Idriss IM, Boulanger RW (2006) Semi-empirical procedures for evaluating liquefaction potential during earthquakes. Soil Dyn Earthq Eng 26:115–130

Idriss IM, Boulanger RW (2008) Soil liquefaction during earthquakes. Earthquake Engineering Research Institute, Oakland

Kamai R, Boulanger RW (2013) Simulations of a centrifuge test with lateral spreading and void redistribution effects. ASCE J Geotech Geoenviron Eng 139(8):1250–1261

Kawashima K, Takahashi Y, Ge H, Wu ZS, Zhang JD (2009) Reconnaissance report on damage of bridges in 2008 Wenchuan, China, earthquake. J Earthq Eng 13(7):965–996

Kayen R, Moss RE, Thompson EM, Seed RB, Cetin KO, Kiureghian DA, Tanaka Y, Tokimatsu K (2013) Shear-wave velocity-based probabilistic and deterministic assessment of seismic soil liquefaction potential. ASCE J Geotech Geoenviron Eng 139(3):407–419

Khoshnevisan S, Juang H, Zhou YG, Gong WP (2015) Probabilistic assessment of liquefaction-induced lateral spreads using CPT-Focusing on the 2010-2011 Canterbury earthquake sequence. Eng Geol 192:113–128

Li J, Peng T, Xu Y (2008a) Damage investigation of girder bridges under the Wenchuan earthquake and corresponding seismic design recommendations. Earthq Eng Eng Vib 7(4):337–344

Li XJ, Zhou ZH, Huang M, Wen RZ, Yu HY, Lu DW, Zhou YN, Cui JW (2008b) Preliminary analysis of strong-motion recordings from the magnitude 8.0 Wenchuan, China, earthquake of 12 May 2008. Seismol Res Lett 79(6):844–854

Mello UT, Pratson LF (1999) Regional slope stability and slope-failure mechanics from the two-dimensional state of stress in an infinite slope. Marine Geo 154(1–4):339–356

Modoni G, Flora A, Mancuso C, Tatsuoka F (2000) Evaluation of gravel stiffness by pulse wave transmission tests. Geotech Test J 23(4):506–521

Rollins KM, Evans MD, Diehl NB, Daily WD (1998) Shear modulus and damping relationships for gravels. ASCE J Geotech Geoenviron Eng 124(5):396–405

Seed HB, Seed RB, Harder LF, Jong HL (1989) Re-evaluationof the lower San-Fernando Dam. Report 2: Examination of the post-earthquakeslide of February 9, 1971. Contract Report GL-89-2, Dept. of Army, U.S. ArmyWar. Exp. Sta., Vicksburg, MS

Toyota H, Takada S (2019) Effects of gravel content on liquefaction resistance and its assessment considering deformation characteristics in gravel-mixed sand. Can Geotech J 56(12):1743–1755

Trifunac MD, Brady AG (1975) A study on the duration of strong earthquake ground motion. Bull Seismol Soc Am 65(3):581–626

Wilkinson S, Grant D, Williams E, Paganoni S, Fraser S, Boon D, Mason A, Free M (2013) Observations and implications of damage from the magnitude M_w6.3 Christchurch, New Zealand earthquake of 22 February 2011. Bull Earthq Eng 11(1):107–140

Yang J, Sze HY (2011) Cyclic behaviour and resistance of saturated sand under non-symmetrical loading conditions. Geotechnique 61:59–73

Yegian MK, Ghahraman VG, Harutiunyan RN (1994) Liquefaction and embankment failure case histories, 1988 Armenia earthquake. ASCE J Geotech Eng 120(3):581–596

Zhou YG, Chen YM (2007) Laboratory investigation on assessing liquefaction resistance of sandy soils by shear wave velocity. ASCE J Geotech Geoenviron Eng 133(8):959–972

Zhou YG, Chen YM, Ling DS (2009) Shear wave velocity-based liquefaction evaluation in the great Wenchuan earthquake: a preliminary case study. Earthq Eng Eng Vib 8(2):231–239

Zhou YG, Liu K, Ling DS, Shen T, Chen YM (2018) Threshold seismic energy and liquefaction distance limit during the 2008 Wenchuan earthquake. Bull Earthq Eng 16(11):5151–5170

Zhou YG, Xia P, Ling DS, Chen YM (2020) Liquefaction case studies of gravelly soils during the 2008 Wenchuan earthquake. Eng Geol 274:105691